Correlation of Microstructure and Fracture Toughness in Three High-Speed Steel Rolls

SUNGHAK LEE, KEE-SUN SOHN, CHANG GIL LEE, and BYUNG IL JUNG

The objective of this study is to clarify the fracture characteristics of high-speed steel (HSS) rolls in terms of microstructural factors such as matrix phase and primary carbide particles. Three HSS rolls with different chromium contents were fabricated by centrifugal casting, and the effect of the chromium addition was investigated through microstructural analysis, fracture-mechanism study, and toughness measurement. The hard and brittle primary carbides, as well as the eutectic carbides (ledeburites), were segregated in the intercellular regions and dominated overall properties. Observation of the fracture process revealed that these primary carbides cleaved first to form microcracks at low stress-intensity factor levels and that the microcracks then readily propagated along the intercellular networks. The addition of chromium to a certain level yielded microstructural modification, including the homogeneous distribution of primary carbides, thereby leading to enhancement of fracture toughness of the HSS rolls.

I. INTRODUCTION

HIGH-speed steel (HSS) is a highly alloyed, very hard steel used mostly for cutting metals at ''high speed.''[1,2,3] In recent years, HSS has been used for roll materials, since it has several inherent advantages over conventional roll materials, such as excellent hardness, strength, fracture toughness, wear resistance, and thermal-fatigue life, as well as a fine and stable microstructure. The HSS retains its shape for a prolonged time, offering a good opportunity to produce high-quality rolls during a high-temperature operation. The HSS rolls usually contain vanadium for increased abrasion resistance, chromium for increased oxidation resistance and hardness, and molybdenum and tungsten for carbide formation and red hardness.[1,2,4] Sometimes cobalt is added for improved high-temperature hardness.[5,6,7]

The properties of HSS rolls are critically dependent upon the type and hardness of carbides, which are either primary carbides formed during solidification, or secondary carbides precipitated from solid solution during tempering.[5,8–10] It has been reported that most of the primary carbides are distributed mainly along intercellular boundaries formed during solidification and are retained even in the finished product, which may result in low fracture toughness and thermal-fatigue life.[7,8] Thus, the advantages offered by HSS for high-quality roll design may be fully realized only with an understanding of the microstructural evolution and its effect on the mechanical properties, especially on fracture toughness.

SUNGHAK LEE, Associate Professor, and CHANG GIL LEE, Postdoctoral Research Associate, are with the Center for Advanced Aerospace Materials, Pohang University of Science and Technology, Pohang, 790-784 Korea. KEE-SUN SOHN, formerly Research Assistant, Center for Advanced Aerospace Materials, Pohang University of Science and Technology, is Postdoctoral Research Associate, Department of Materials, Queen Mary and Westfield College, University of London, London, E1 4NS United Kingdom. BYUNG IL JUNG, General Manager, is with the Roll Technology Department, Kangwon Industries, Ltd., Pohang, 790-370 Korea.

Manuscript submitted September 19, 1995.

In this study, commercially produced HSS rolls were investigated, with close attention to (1) the fracture mechanism, (2) the role of microstructural factors on fracture process, and (3) the effect of chromium content on microstructural modification. A scanning electron microscope (SEM), as well as an optical microscope, was used for the microstructural observation and fracture-mechanism analysis. The SEM sample stage was designed for *in situ* examination of the fracture process and acquisition of apparent fracture-toughness data.[11]

II. EXPERIMENTAL

Three HSS rolls were produced by a vertical centrifugal casting route at Kangwon Industries, Ltd. (Pohang, Korea) as a finished roll product. They have a basic composition of 1.5C-0.5Mn-1Si-1Ni (wt pct), along with about 10 wt pct of strong carbide formers such as molybdenum and vanadium. The chromium contents were controlled to be 3.5, 5.5, and 8.0 pct (Table 1). The samples in this study were obtained from the shell part of the three HSS roll products and are referred to as roll A, roll B, and roll C, respectively. The samples were austenitized at 950 °C to 1050 °C for 1 hour and air cooled, followed by a double-tempering treatment at about 500 °C to 600 °C. The purpose of this double tempering was to obtain a totally martensitic matrix, by transforming the retained austenite to martensite with the first temper and then to tempered martensite with the second temper.

Microstructures of the HSS rolls were observed by an optical microscope and an SEM. An image-processing system was used for the quantitative analysis of the cell size and the distribution of primary carbides. In order to identify the carbide type, backscattered electron imaging and energy-dispersive X-ray spectroscopy (EDS) were also used. Microvickers hardness testing was conducted on individual phases and the data acquired were related, with the identity of carbides determined by the microscopy. For measuring hardness of very hard phases, a load of 5 g was used.

The *in situ* SEM fracture test for direct observation of the fracture process was performed at room temperature

Table I. Chemical Composition of the Shell Part of the HSS Rolls Used (Weight Percent)

Roll	C	Mn	Si	P	S	Cr	Ni	Mo	V	Fe
A	1.72	0.80	0.94	0.02	0.008	3.51	1.17	3.03	4.40	bal
B	1.80	0.81	0.96	0.02	0.006	5.58	1.15	3.06	4.45	bal
C	1.80	0.83	0.92	0.03	0.008	8.07	1.12	3.10	4.60	bal

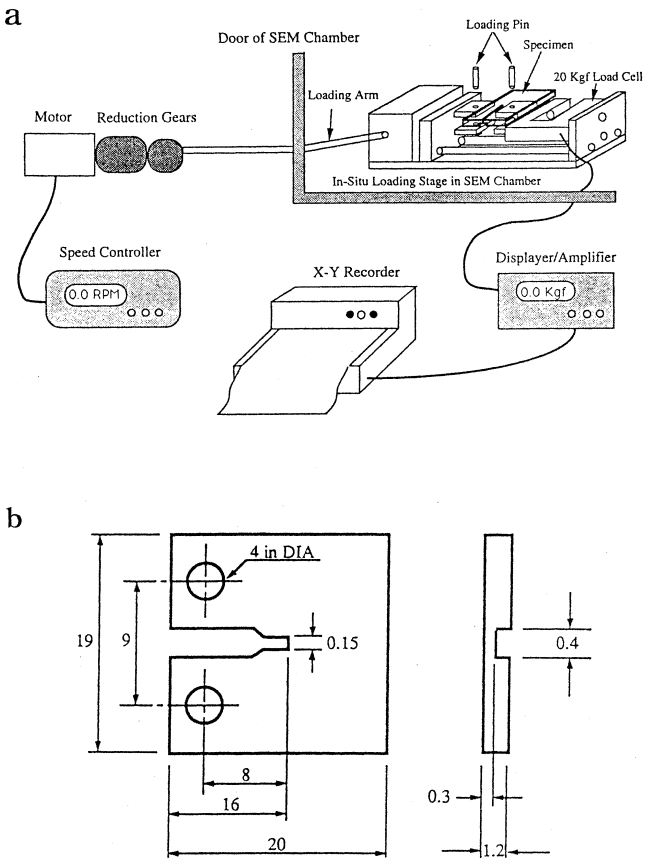

Fig. 1—(*a*) The CT type loading stage used for *in situ* observation and measurement of apparent fracture toughness; which was inserted into the SEM vacuum chamber. (*b*) The shape and dimensions of the small and thin CT type specimen (unit: mm).

using a specially designed loading stage (Figure 1(a)).[11] The loading stage was inserted into the vacuum chamber, replacing the standard sample stage. Thin compact-tension (CT) type specimens, whose dimensions were 19 by 20 mm with a thickness of 0.3 mm in the grooved section, were used in this test (Figure 1 (b)). A notch was electrodischarge machined to an actual notch-tip radius of about 75 μm. To develop cracks, load was applied to the specimen after the polished and etched CT specimen was mounted on the stage with the loading pins. Precise control of the loading arm under high torque could be achieved using an external gear system composed of a motor and two reduction gears, with a constant loading speed of 10 to 10^3 μ/min. Micrographs were taken of the specimen surface with loading paused. The value of the stress-intensity factor could be measured at each loading step, by monitoring the applied load using a load cell. The signal from the load cell was amplified and then recorded with the X-Y recorder.

The apparent fracture toughness could be measured using the *in situ* loading stage and the CT specimen with a sharp notch. A sharp notch instead of a fatigue crack was used because of the difficulty in preparing a fatigue precrack in very brittle material. In addition, it has been reported that when the sharp-notched specimens (tip radius of 30 to 70 μm) are used, apparent fracture toughness is nearly identical to fracture toughness, K_{IC}, in brittle materials such as ultra-high-strength steels and metal-matrix composites.[12–15] A load-time curve instead of a load-displacement curve was obtained at the loading speed of 30 μm/min. Test and data-interpretation procedures followed ASTM E399 specifications.[16] From the aforementioned methods, the maximum load in the load-time curve was considered to be P_Q. This seems reasonable, because brittle materials such as HSS show little plastic behavior. None of the test values satisfy the ASTM requirement for minimum specimen thickness (the calculated minimum thickness is about 3 mm). Thus, the toughness values obtained from the aforementioned test are not K_{IC} values, but rather are K_C values that depend on the specimen thickness. After the fracture test, fracture surfaces of the CT specimens were examined to compare the fracture behavior in the polished surface region and throughout the thickness.

III. RESULTS

A. *Microstructure*

The optical micrographs of the three HSS rolls (Figures 2(a) through (c)) show that the coarse primary carbides are mostly located in the intercellular regions, forming continuous networks of densely populated carbides. They also reveal that the solidification cell sizes are 20 to 40 μm.

Figures 3(a) through (c) are SEM micrographs of the three rolls, showing fine spherical carbides in the tempered martensite matrix. Here again, the change of martensite type from plate type (roll A) to lath type (roll C) can be confirmed from the observed matrix structure. The carbon contents in the matrices were determined from the quantitative wavelength dispersive spectroscopy (WDS) and are listed in Table II. The carbon contents are increased in the order of roll C, roll B, and roll A, reflecting the change of the tempered martensite type. Fine spherical carbides are observed in the matrices of roll B and roll C, and the average size in roll C is somewhat larger than that in roll B, while the carbides are rare in roll A. In order to find the origin of these spherical carbides, an HSS roll was fabricated by a small-scale horizontal-type centrifugal casting, and its chemical composition is 1.9C-1.6W-1.7Mo-5.5Cr-5.1V-0.7Si-0.3Mn-1.0Ni. Figures 4(a) through (c) are the as-cast, the as-austenitized, and the tempered microstructures of the roll, respectively. A number of fine spherical carbides exist in the as-cast structure, and were retained without a change in their size and shape after tempering treatment. Thus, it can be concluded that fine spherical carbides distributed in the matrix are not secondary carbides formed during tempering, but rather are a sort of primary carbide formed during slow air cooling after casting (the air cooling usually takes 1 or 2 days because of the very large roll size). The EDS spectrum of the carbides is shown in Figure 4(d), although it includes the matrix composition due to the size of the fine carbides. From this spectrum, fine spherical carbides are identified by the EDS analysis to be chromium-rich carbides.

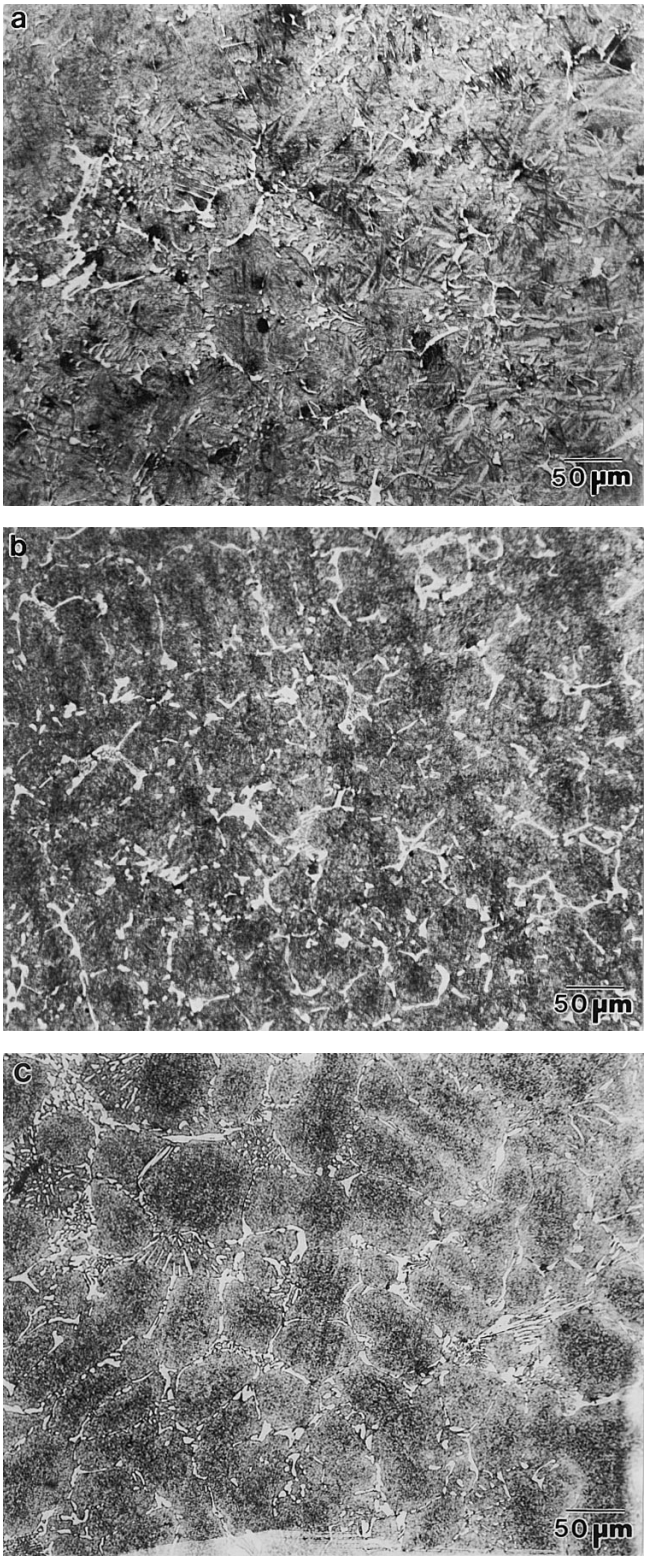

Fig. 2—Optical micrographs of the shell region for (*a*) roll A, (*b*) roll B, and (*c*) roll C.

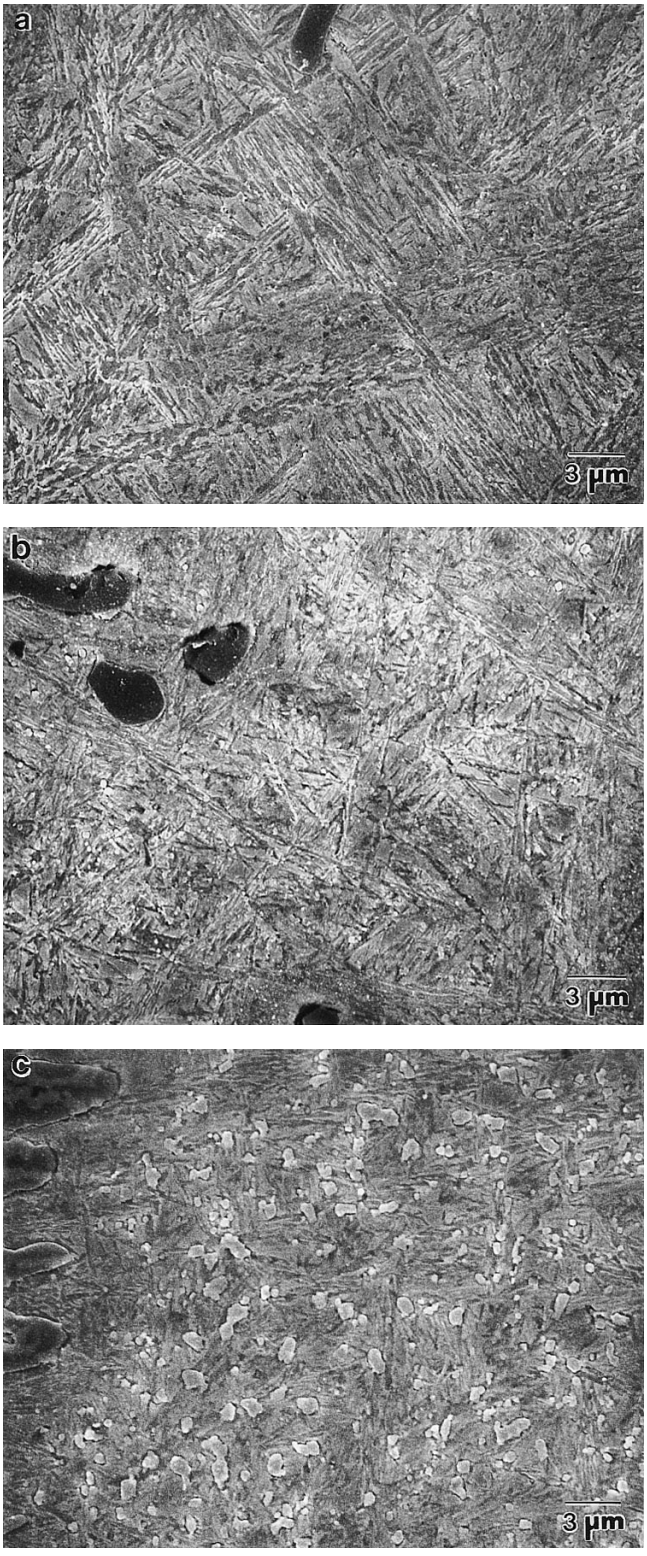

Fig. 3—SEM micrographs of (*a*) roll A, (*b*) roll B, and (*c*) roll C.

Table II. Carbon Content in the Matrix Obtained from WDS Analysis (Weight Percent)

Roll	Carbon Content (Pct)
A	0.59
B	0.55
C	0.30

As the quantitative data (Table III) show, the solidification cell size of roll B is smaller than those of roll A and roll C. Also, the primary carbides in roll B are smaller and more spherical than those in the other two rolls. However, the volume fractions of the primary carbides in the three rolls are comparable, ranging from 10 to 13 pct. In addition

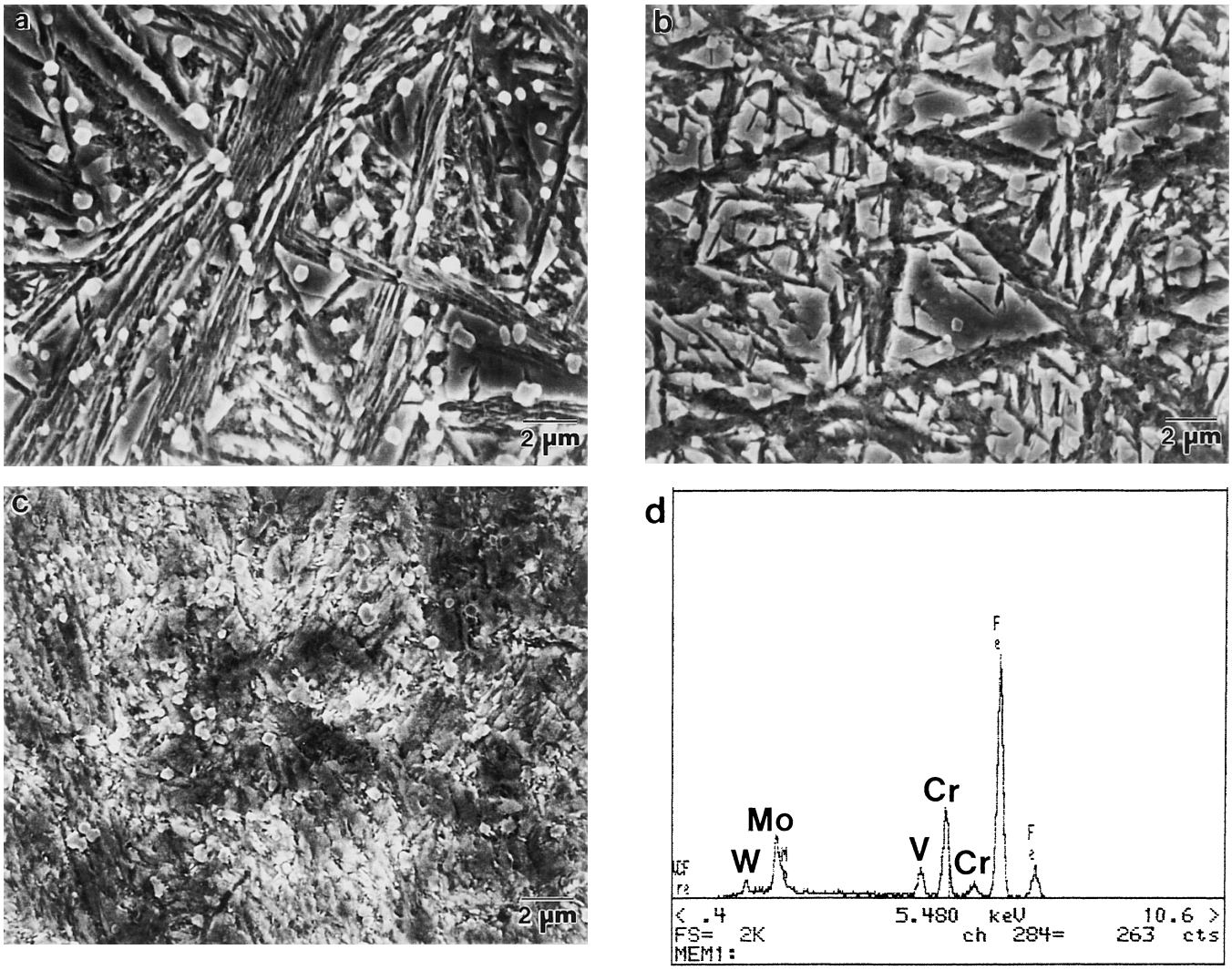

Fig. 4—SEM micrographs of (*a*) the as-cast, (*b*) the as-austenitized, and (*c*) the as-tempered HSS roll fabricated by a small-scale horizontal-type centrifugal casting, showing fine spherical carbides in the matrix. (*d*) An EDS spectrum of fine spherical carbides.

Table III. Results of Quantitative Metallographic Analysis as Determined from SEM Micrographs

	Average Size (μm)			Aspect Ratio	Volume Fraction (Pct)	
Roll	Cell	Primary Carbide	Eutectic Carbide	of Primary Carbides	Primary Carbide	Eutectic Carbide
A	33.9	3.7	3.2	3.5	10.3	1.7
B	22.7	4.0	3.4	1.4	10.1	1.7
C	38.6	6.0	5.4	2.9	13.1	4.2

to the coarse primary carbides, other types of carbides also exist in the intercellular region. Figures 5(a) through (c) show eutectic carbides, whose shape is like a fish bone or a flower. These eutectic carbides are usually located at a cell boundary or triple junction. Roll C has the largest amount of eutectic carbide (Table III).

The three types of primary carbides, *i.e.*, molybdenum-, chromium-, and vanadium-rich, are marked by M, C, and V in Figure 6(a), and shown by the EDS spectra of Figures 6(b) through (d), respectively. Also, eutectic carbides shown in Figures 5(a) through (c) are identified by the EDS analyses to be chromium- and molybdenum-rich carbides.

B. *Hardness*

Microvickers hardnesses measured at various positions are listed in Table IV. The matrix hardness values are roll A, roll B, and roll C, in decreasing order. The hardnesses of the intercellular primary carbides are as high as 3000. The coarse carbides in the cell interior have hardnesses over 2500. On the other hand, the hardness value of the eutectic carbides ranges from 850 to 900, which is much lower than that of the primary carbides. The overall hardness values were measured using a load of 10 kg and were found to be decreasing, in the order roll B, roll A, and roll C. Rockwell (*C* scale) hardnesses (R_C) were also measured and are included in Table IV. The R_C values have the similar trend of the overall vickers hardness.

C. *In Situ Observation of Microfracture Process*

The *in situ* fracture-initiation process of roll B is shown in Figures 7(a) through (d). Figure 7(a) is the microstructure

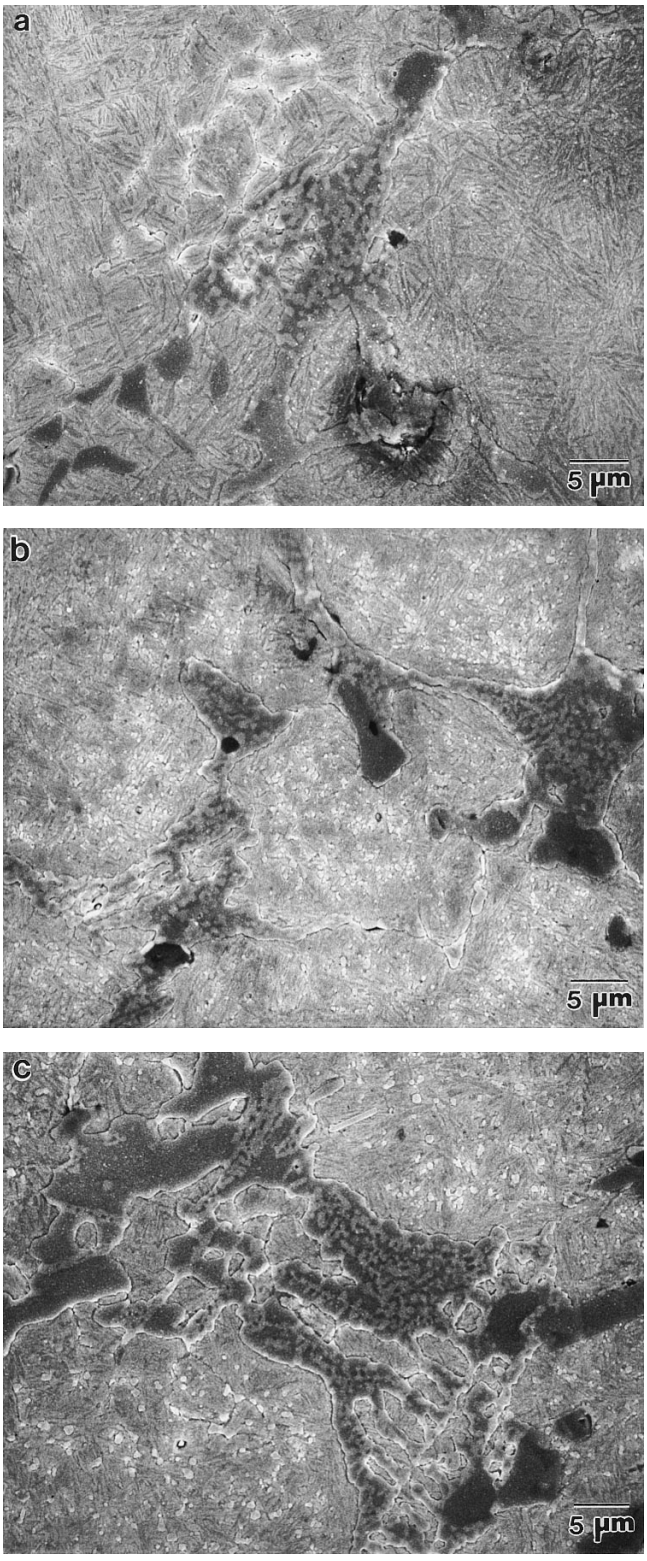

Fig. 5—SEM micrographs of (*a*) roll A, (*b*) roll B, and (*c*) roll C, showing eutectic carbide structure.

of the notch-tip region before loading and shows the intercellular network structure of primary carbides. At the initial stage of loading, microcracks initiate either at the primary carbides or at the interface between the primary carbides and the tempered martensitic matrix, as marked by arrows in Figure 7(b). The stress-intensity factor (K_I) was measured to be 34.8 MPa$\sqrt{m}$. With further loading (K_I = 35.1 MPa$\sqrt{m}$), some carbides cleave to form microcracks. The cracks preferentially propagate into adjacent carbides and/or carbide/matrix interfaces along the intercellular networks to form discontinuous cracks of 10 to 20 μm in length (Figure 7(c)). Although these brittle cracks stop growing temporarily when they meet the relatively ductile matrix, they eventually connect (Figure 7(d)).

In comparison with roll B, roll A exhibits a more or less brittle crack-opening process (Figures 8(a) through (c)). Coarse primary carbides are more segregated along cell boundaries, and have a more rodlike shape, compared with the equiaxed shape in roll B, as indicated by aspect ratios in Table III. However, their volume fraction and size are comparable to those of roll B and roll C. The cracking process is similar to roll B, *i.e.*, microcracks are formed at the carbide/primary interface or at the primary carbides (Figures 8(a) and (b)). The microcracks propagate to the nearby intercellular carbides at additional loading (Figure 8(c)). Note that microcracks in roll A are somewhat longer (30 to 50 μm) than those in roll B, and propagate in a more brittle manner, attributable largely to the shorter matrix region between primary carbides.

Figures 9(a) through (d) show the fracture process of roll C. At a relatively low stress-intensity level (K_I = 29.2 MPa$\sqrt{m}$), the crack initiation and propagation along intercellular boundaries occur catastrophically in the notch-tip region, to form a very long crack of about 200 μm in length (Figure 9(a)). Although the fracturing behavior of roll C is similar to that of roll A or roll B, the remote stress required for local fracture of primary carbides is quite low. Further observation of the fracture process in front of a propagating crack is made with reference to a series of SEM micrographs in Figures 9(b) through (d), showing a series of brittle cracks formed by fracturing of primary carbides or by separation of the carbide/matrix interface and their propagation path along the cell boundary.

Figures 10(a) through (c) are fracture surfaces of the *in situ* fracture specimens. Fracture mode is mostly quasicleavage, together with limited regions of ductile dimpled fracture (labeled by *D*'s). Note that the amount of ductile fracture on fracture surfaces is largest in roll B, as a result of the more homogeneous distribution of primary carbides.

D. *Fracture Properties*

As described in Section II, the apparent fracture-toughness values, K_C, were determined with the *in situ* SEM fracture technique and are listed in Table V. For comparison, the apparent fracture-toughness values obtained from thin CT specimens with a sharp crack and the plane-strain fracture-toughness values that satisfy ASTM thickness requirements are also listed. All the test data are averaged values taken from two or more specimens. The toughness values are increasing, in the order roll C, roll A, and roll B. The toughness values of the thin specimens with a sharp crack are comparable to those of the thin specimens with a sharp notch, in good agreement with the statement in Section II.[12–15] However, neither specimen satisfies the plane-strain condition. When the toughness obtained from the thin specimen (plane-stress condition) is compared with the plane-strain fracture toughness of the bulk specimen for roll

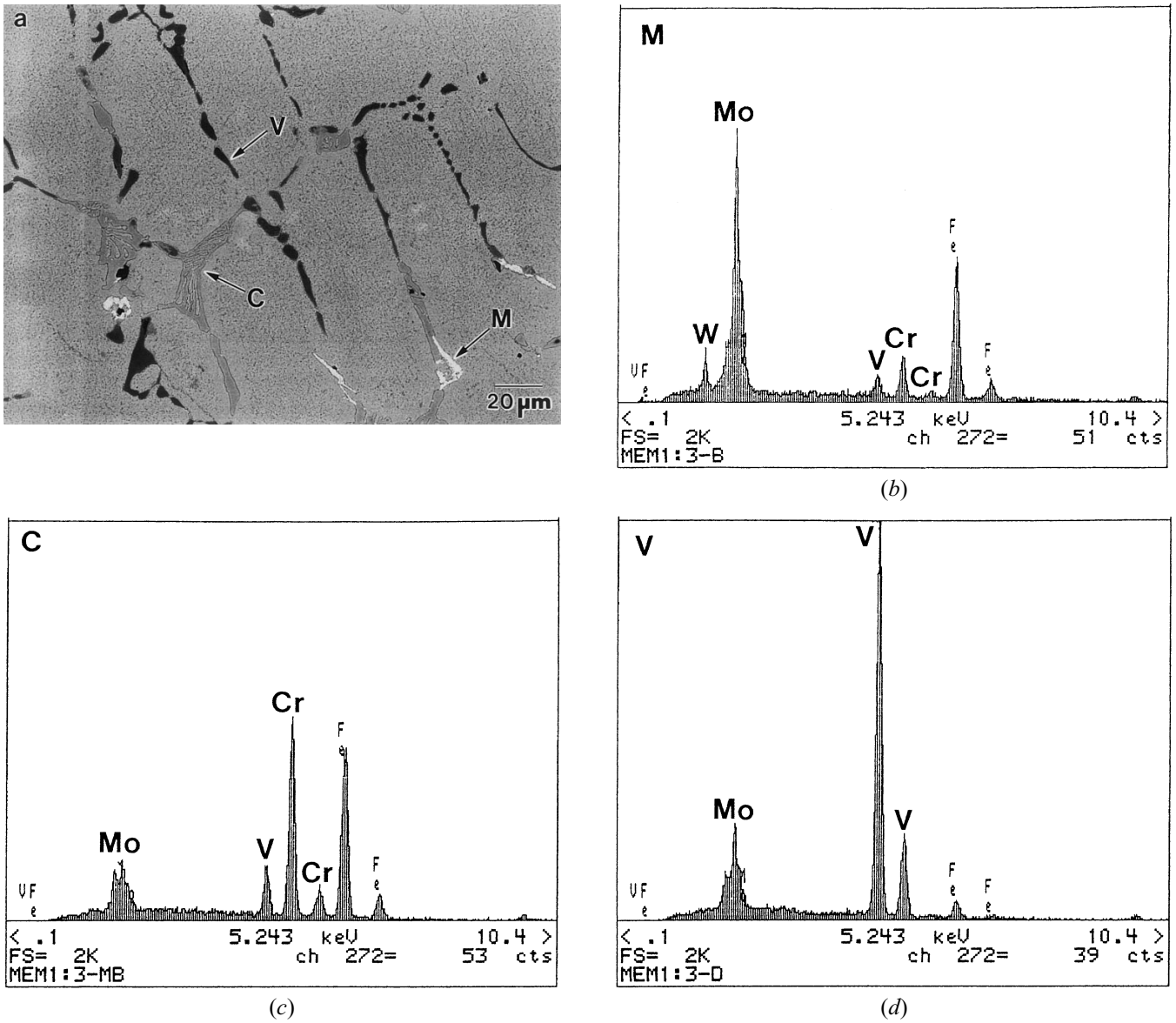

Fig. 6—(*a*) Backscattered electron image of roll C, (*b*), (*c*), and (*d*) EDS spectra of the *M*, *C*, and *V* regions marked in (*a*), respectively.

Table IV. Vickers Hardness Test Results (Load: 5 g)

Location of Indentation	Vickers Hardness Number		
	Roll A	Roll B	Roll C
Matrix	756	693	639
Primary carbides			
on cell boundary	3126	3100	3077
within cell	2576	—	2723
Ledeburite	—	892	856
Overall structure*	706	725	681
Overall structure**	60	61	59

*Measured by the applied load of 10 kg.
**Measured Rockwell hardness (C scale) values.

B, the former is slightly higher than the latter. This is the trend between plane-strain and plane-stress conditions in fracture-toughness testing, but the difference is relatively small in the brittle HSS roll. The fracture toughness of ductile materials in the plane-strain condition is one-third to one-half of the toughness in the plane-stress condition.[17,18] Furthermore, the macroscopic fracture mode observed in the fractured thin CT specimens (Figures 10(a) through (c)) shows a flat surface, rather than a slant surface or a shear lip. The flat surface is an indication of a plane-strain condition,[17] while the slant surface is a typical fracture mode in a plane-stress condition.

IV. DISCUSSION

A. *Microstructural Evolution*

All the microstructural evolution of the HSS rolls has been explained in terms of the chromium content, which can be summarized as follows: (1) The fine spherical carbides increase from none (roll A) to a high density (roll C). (2) The eutectic carbide volume fraction increases with increasing chromium content. (3) The matrix phase changes from totally plate-type tempered martensite (roll A) to the complete disappearance of plate-type tempered martensite (roll C). (4) The distribution of primary carbides is the best

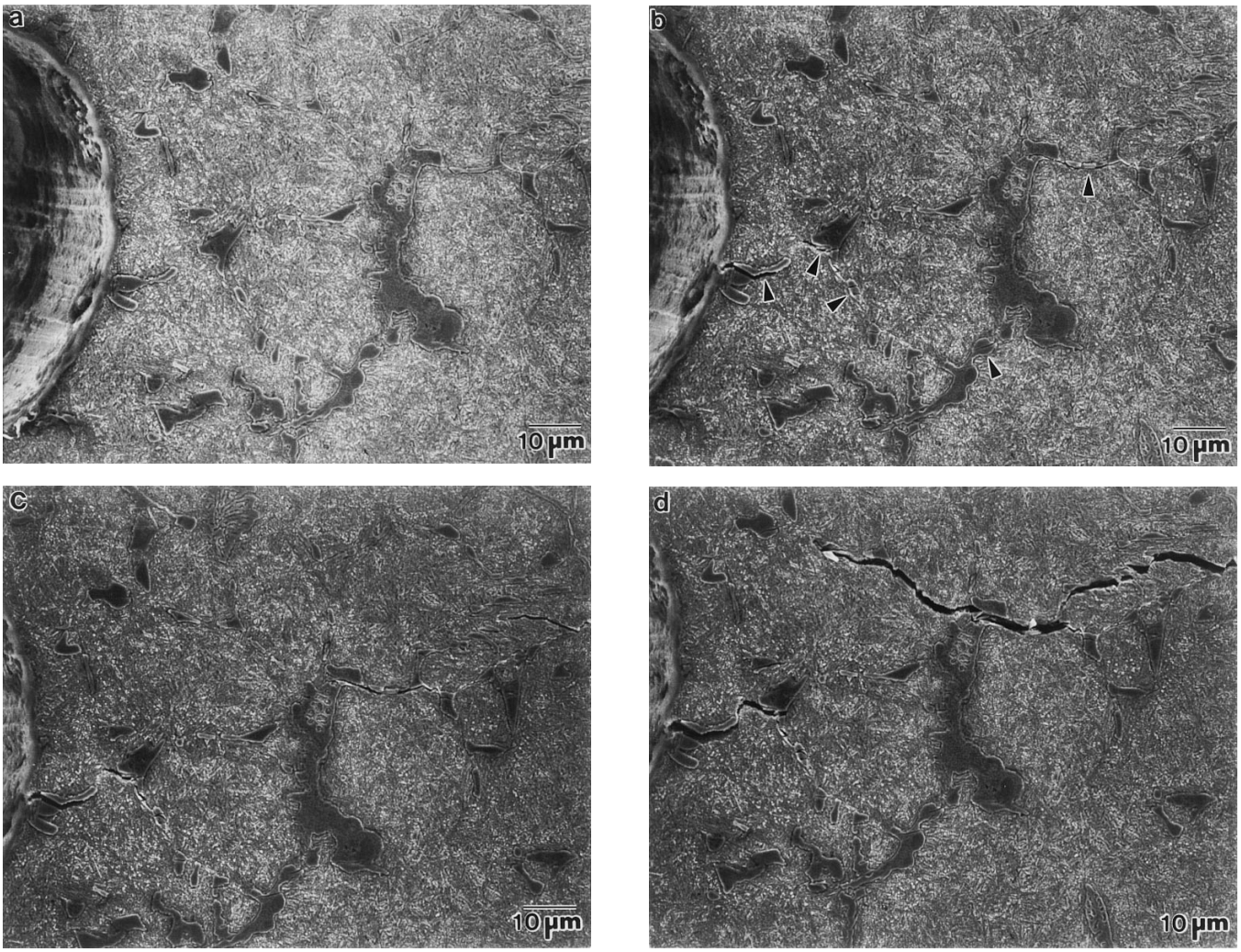

Fig. 7—A series of SEM micrographs near a notch tip of roll B, showing (*a*) basic SEM microstructure (K_I = 0 MPa), (*b*) microcrack formation at primary carbide/matrix interfaces under the relatively small load (K_I = 34.8 MPa), (*c*) and (*d*) crack propagation along the intercellular networks (K_I = 35.1 and 35.2 MPa , respectively).

at the medium level of chromium (roll B), with little change in the volume fraction.

Even though the mechanism of formation is not readily determined, the increased population of the fine spherical chromium-rich carbides with increasing chromium content indicates that the chromium addition over a certain level promotes the formation of the fine carbides in, the HSS rolls. Clearly, from the microstructural analyses, chromium plays a role in forming the eutectic and the fine spherical carbides by combining with carbon. For example, the large amount of the eutectic and the fine carbides in roll C (Table III) result from the high content of chromium, which promotes the eutectic reaction during solidification and the formation of the fine carbides during cooling. In this case, the smaller amount of carbon remains in the matrix (Table II), and thus the matrix consists mainly of lath-type tempered martensite instead of plate-type martensite. It is known that the decrease of carbon content changes the martensite type from plate to lath. A sample that contains a carbon content lower than 0.4 pct, like roll C, has lath-type martensite on quenching, whereas plate-type martensite is the major phase when the carbon content is higher than 0.4 pct.[2] Conversely, in the case of roll A, which contains the low chromium content, a few eutectic and fine carbides are formed, and subsequently the matrix is composed of plate-type tempered martensite because of the higher carbon content in the matrix. Therefore, addition of chromium results in a complete plate-type tempered martensitic matrix without fine spherical carbides in roll A, a matrix of plate-type and lath-type tempered martensite with some fine carbides in roll-B, and a lath-type tempered martensite matrix with a large number density of fine carbides in roll C. In this way, the chromium content plays an important role in determining the properties of the matrix.

The chromium effect on the composition of the primary carbides might be minimal. The change in the morphology of the primary carbides is believed to be a result of the matrix modification by chromium rather than the direct effect of chromium on the primary carbides.

B. *Hardness*

The hardness of the intercellular primary carbides is about 3000, indicating that they are MC-type vanadium-rich carbides that can affect the overall hardness and the wear resistance. The coarse carbides in the cell interior have

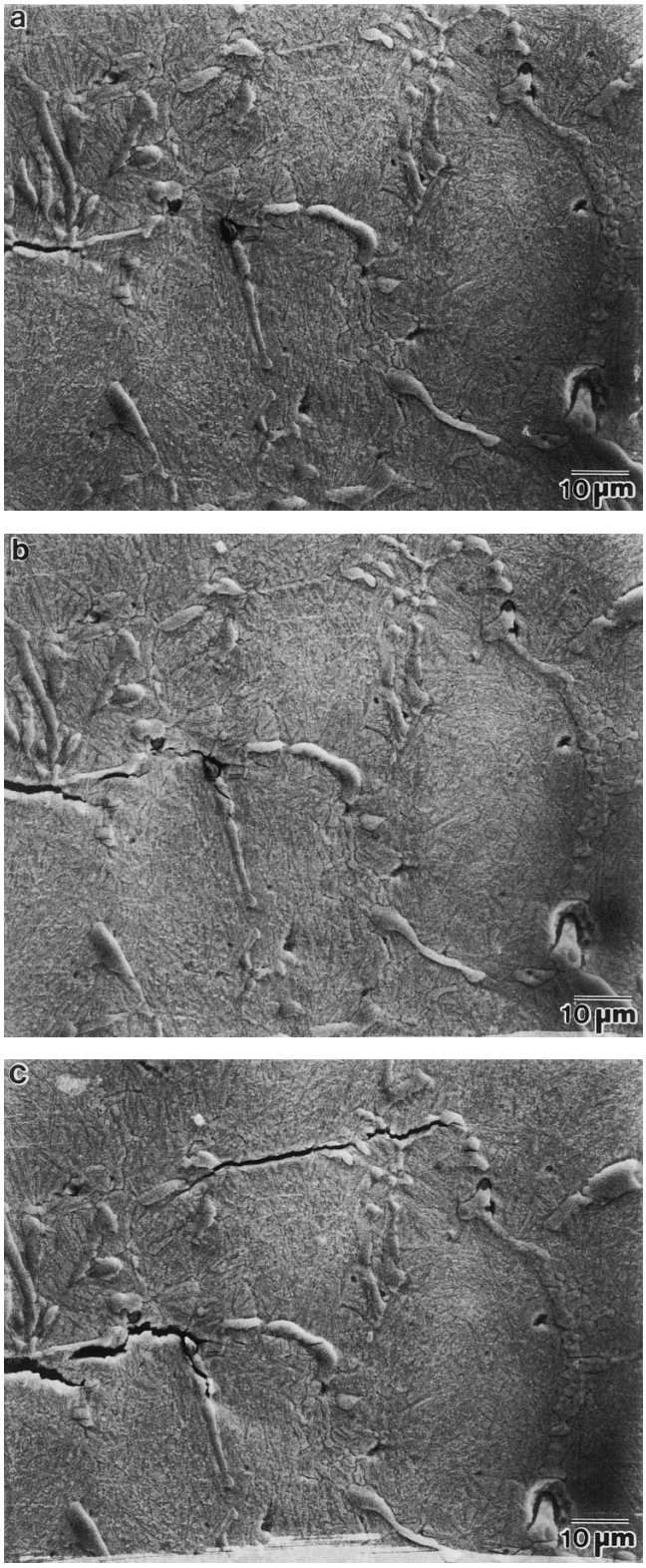

Fig. 8—A series of SEM micrographs in front of a propagating crack of roll A, showing (*a*) and (*b*) microcrack formation at primary carbide/matrix interfaces and primary carbides and (*c*) crack propagation along intercellular boundaries.

hardnesses over 2500, so that they are another MC-type vanadium-rich carbide. On the other hand, the hardness value of the eutectic carbides ranges from 850 to 900, which is much lower than that of the primary MC-type carbides. This hardness range suggests that the eutectic carbides are a mixture of molybdenum-rich M_2C-type carbides and chromium-rich M_6C-type carbides.[19,20] The mixture structure of the eutectic carbide is also reasonably accepted by the carbide decomposition to M_2C and M_6C carbides during austenitization, whose reaction rate depends on time and temperature.[8].

The fact that roll C contains the largest amount of fine spherical carbides and displays the lowest hardness suggests that the amount of fine chromium-rich carbides is not important in determining the matrix hardness. The trend of hardness is well correlated with the amount of primary carbides and the characteristics of the matrix (Table IV). However, some of the phenomenology is not so clearly explained. For example, it is not obvious why the overall hardness of roll B is higher than that of roll A, which has the harder matrix. Since the volume fractions of the primary carbides are nearly identical for both rolls, an inverse relationship of hardness is expected. It is believed that the high hardness value of roll B is attributable to the more uniform distribution of the hard primary carbides. The fact that roll C, whose carbides are mostly segregated, displays the lowest hardness is in line with this argument. This can also be explained as a Hall–Petch-type grain (or cell) size effect,[21] since the cell size of roll B is roughly half of that of roll C.

C. *In Situ Fracture Technique*

The *in situ* fracture technique employed in this study has been crucial and efficient for the observation of the fracture process and for the interpretation of the microstructural effects on fracture mechanism. Also, this *in situ* SEM technique has been designed for the measurement of apparent fracture toughness. Since the fracture-toughness results indicate that the technique has some inherent weakness in using a sharp notch introduced to the CT specimen in plane-stress condition, the detailed analyses that describe the notch-tip field in plane-stress *vs* plane-strain condition have to be reconsidered. In spite of this weakness, the difference between the toughness values measured in plane stress *vs* plane strain for the HSS rolls is small (Table V), so that the simple analysis of fracture toughness is reasonable. Thus, this sort of toughness analysis can be applied reasonably to brittle materials such as roll materials, ceramics, metal-matrix composites, and intermetallic compounds. In addition, the analysis technique can also be useful for testing very small or thin samples, a thin coated layer, a surface-treated metallic layer, a metal/ceramic interface, and a welded zone, and for the comparison of fracture-toughness values.

D. *Fracture Mechanism*

The fracture analyses of the HSS rolls are complicated because of the interdependent microstructural factors, which can be classified into two categories: (1) morphology of primary carbides and (2) matrix characteristics.

The microstructural analysis of the HSS rolls found that the primary carbides segregated at the intercellular region consist mostly of vanadium-rich carbides and eutectic carbides (Figures 2(a) through (c). The intercellular structure is particularly pronounced in roll C, whose cell size and volume fraction of primary carbides are the largest (Table

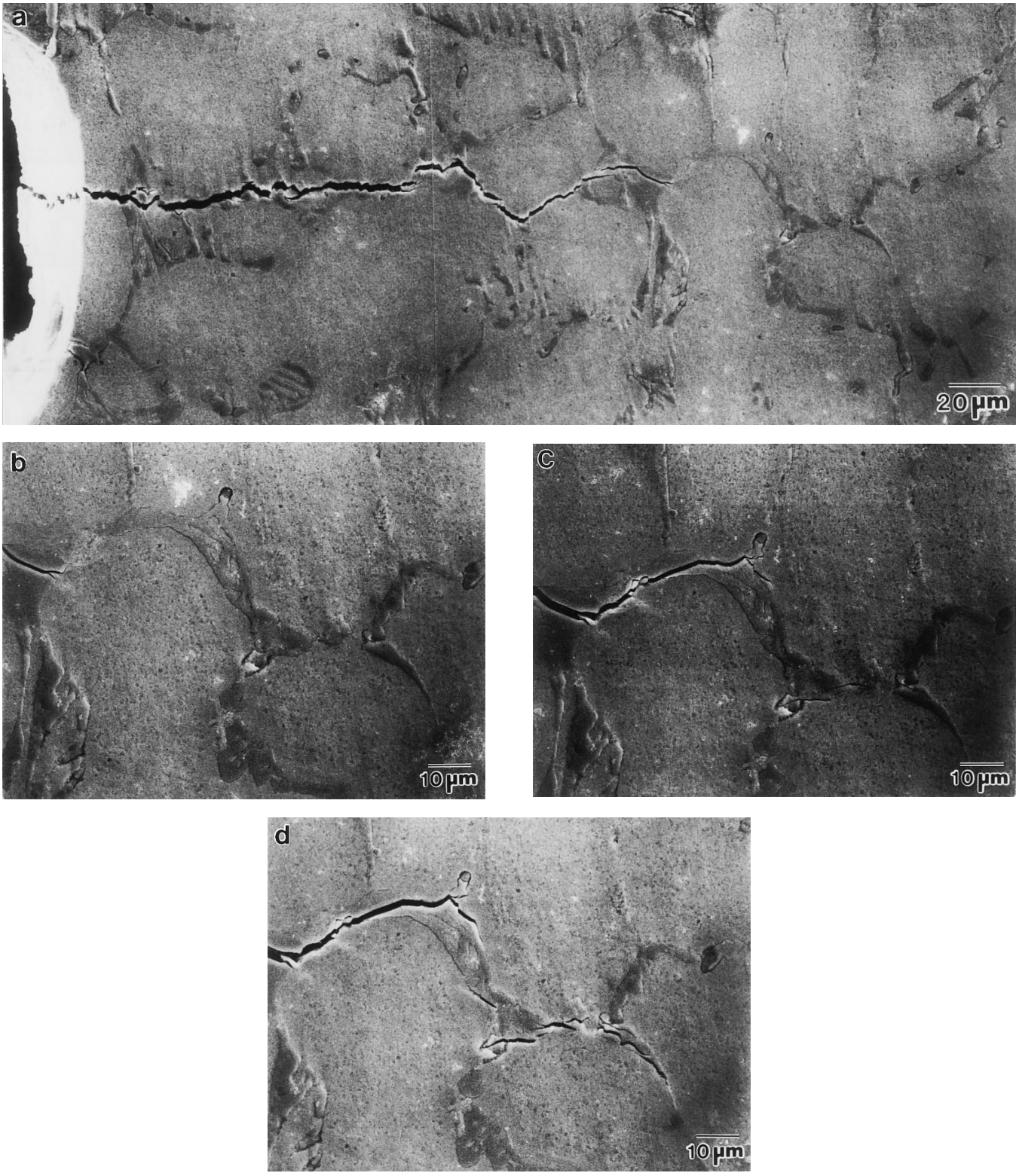

Fig. 9—A series of SEM micrographs near a notch tip of roll C, showing (*a*) catastrophic crack initiation and propagation along intercellular boundaries and (*b*) through (*d*) the further fracture process ahead of the propagating crack in (*a*).

III). It is surmised that this structure is formed by microstructural inhomogeneities caused by interdendritic segregation during solidification, which is unavoidable in cast form and cannot be removed, even when austenitized at a higher temperature.

The HSS rolls are quite different from HSS tools, in that the HSS rolls cannot be hot forged because of their large sizes, whereas the HSS tools are hot forged after casting in order to break the intercellular cast structure. Thus, HSS rolls contain a large number of primary carbides segregated along intercellular boundaries, which can lower the fracture toughness.

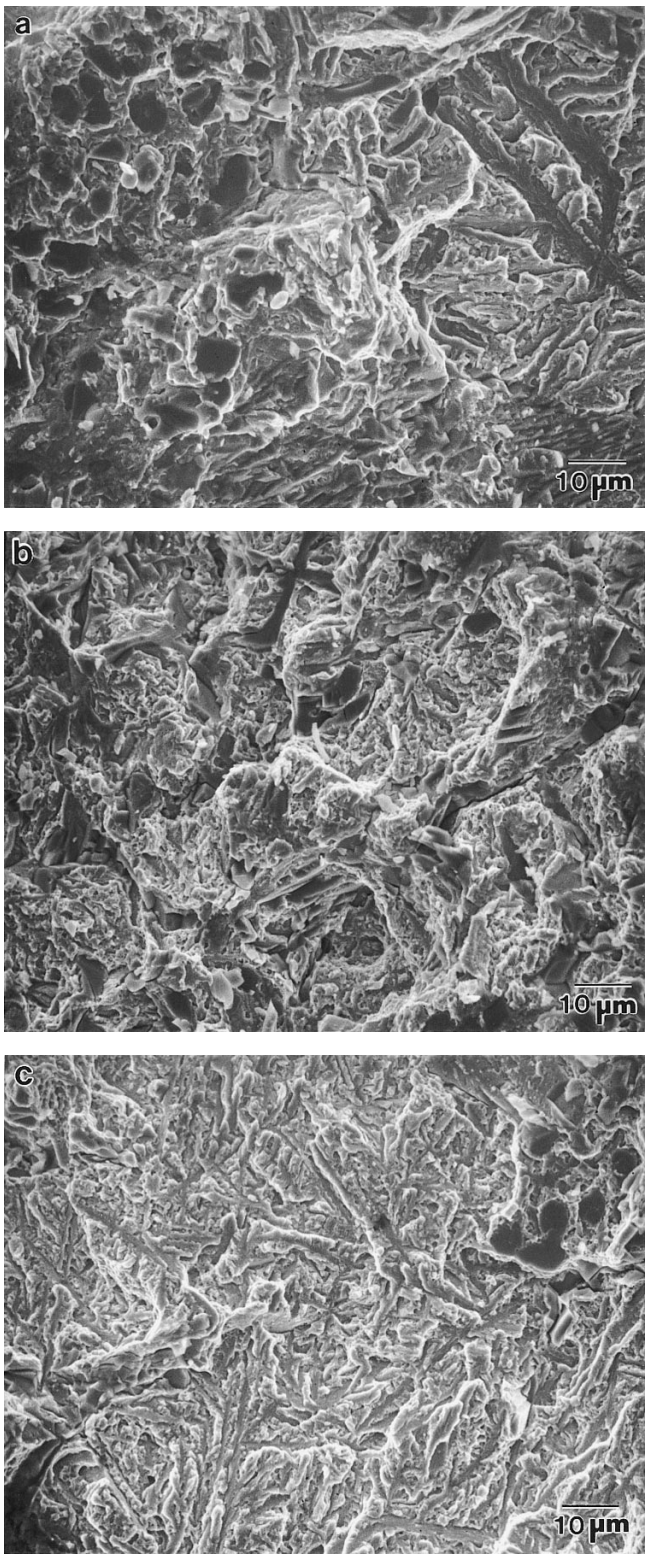

Fig. 10—SEM fractographs of the *in situ* fracture specimens for (*a*) roll A, (*b*) roll B, and (*c*) roll C.

The *in situ* SEM observations show that microcracks are initiated either at the primary carbide/matrix interfaces or by the primary carbides themselves fracturing at relatively low stress levels. It is also observed from Figures 7 through 9 that most of the cracked interfaces or carbides are affected by microcracking of the other carbides when they are in contact or are apart by a short distance. Indeed, the carbides fracture first, and the cracks they cause would subsequently develop the local stress concentration within the high triaxial stress field of a sharp crack tip, leading to cracking of neighboring carbides. From these results, it is evident that the most important event in the fracture-initiation process of the HSS rolls is the brittle cracking of the coarse primary carbides.

Table V. Measured Fracture Toughness Values

Roll	Apparent Fracture Toughness ($MPa\sqrt{m}$) Obtained from: Sharp Notched Specimen	Apparent Fracture Toughness ($MPa\sqrt{m}$) Obtained from: Cracked Specimen	Plane Strain Fracture Toughness Obtained from Sharp Notched Bulk Specimen
A	33.2	34.7	—
B	36.9	34.7	30.8
C	29.7	28.7	—

The fractographs of the *in situ* CT specimens (Figures 10(a) through (c)) show both a quasi-cleavage-type and a dimple-type fracture. The total area fraction of dimple-type fracture is quite small: less than 10 to 20 pct of the overall fracture surface area. It is likely that the quasi-cleavage-type fracture is associated mainly with the primary carbides located along the intercellular region or with interfacial fracture between the carbides and the matrix. In contrast, dimpled fracture takes place when the crack diverges from the intercellular region, or when the crack passes through the matrix, as voids can be formed around relatively fine spherical carbides.

Even though the microcracking of the primary carbides at the initial stage of loading is identical for all three HSS rolls, the subsequent development of cracks leading to fracture is quite different. In roll A and roll C, the microcracks located in the carbide-rich intercellular regions directly cause brittle fracture along the intercellular boundary, resulting in the relatively low fracture toughness in these rolls (Table V). By contrast, in roll B, in which the primary carbides are more spaced, a large matrix ligament between the microcracks formed at the primary carbides is generally found, thereby resulting in a ductile dimpled region on the fracture surface (Figure 10(b)). The ductile matrix serves as an obstacle for the crack propagation. This effect is directly related to the difficulty in initiation and propagation of cracks, as described earlier in Section III–C, and yields the higher value of fracture toughness. Thus, it is apparent that the superior fracture properties of roll B are attributable to the ductile matrix existing even in the intercellular region, although the cracks propagate mostly along a tortuous intercellular fracture path.

The impurity content and level, particularly of S and P, might affect the fracture toughness of the HSS rolls. Since all three rolls investigated in the present study have very low levels of impurity content (Table I), the difference in fracture toughness is primarily attributable to microstructural factors such as primary carbides.

E. *Constituents for High-Quality Roll Design*

The present study has shown that the coarse primary carbides segregated along intercellular boundaries are the most

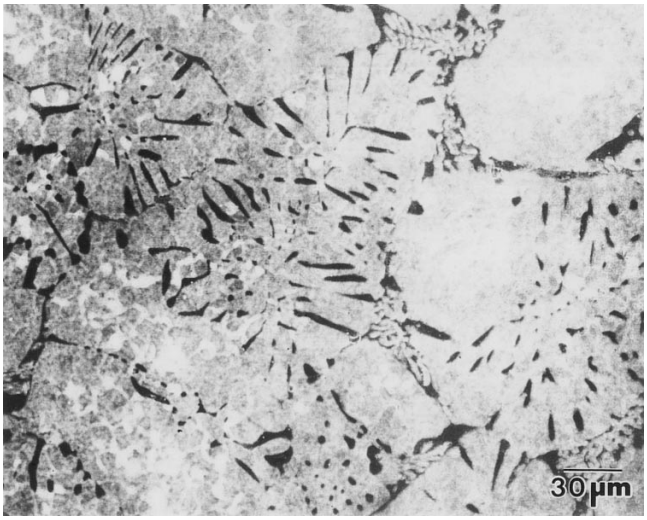

Fig. 11—SEM micrograph of a tungsten-containing HSS roll.

important microstructural factors in determining the fracture properties of the HSS rolls. Vanadium-rich primary carbides are so hard that they are thought to control the overall hardness and the wear resistance of the HSS rolls. Our investigation of the fracture process shows that the distribution of primary carbides, in particular those located in the intercellular region, must be controlled carefully. Therefore, in order to improve the overall mechanical properties, the amount of primary carbides must be increased for wear resistance by the optimization of the ratio of carbon to carbide-forming elements, and homogeneous distribution of the primary carbides must somehow be achieved.

The available information on the effects of process parameters involved in the vertical centrifugal casting is far less than desired for the improvement of mechanical properties and microstructural modification of the HSS rolls. Unless a proper treatment is adopted, the formation of coarse primary carbides during casting is inevitable in conventional casting.

Perhaps the simplest way conceivable for mechanical property improvement of the HSS rolls is the addition of alloying elements such as chromium and tungsten to control the formation of coarse primary carbides. A small addition (2 to 3 wt pct) of tungsten is known to suppress carbide nucleation at the prior cell boundary,[16,19] though the effect of tungsten on the microstructural improvement has yet to be explained. Figure 11 shows an SEM micrograph of a tungsten-containing HSS roll. A number of primary carbides are located at the cell interior, as well as at the intercellular regions, although their volume fraction is increased. From this observation, it is clear that the distribution of primary carbides is improved by the tungsten addition, and thus it is expected to improve mechanical properties. Also, the amount of vanadium must be controlled carefully, since primary vanadium-rich carbides are too hard to match properly to the relatively soft matrix. The divergence of the wear amount between the hard carbides and the matrix might deteriorate the surface profile of the HSS rolls, which is a very important factor governing the surface roughness of the hot-rolled plates.

Another approach to improving mechanical properties is the application of rapid cooling, one of the key casting parameters, for refinement and homogeneous distribution of the primary carbides. The processing variables such as melt superheat, pouring rate, mold rotation speed, and temperature distribution at the shell are all related to the cooling rate and thus have to be optimized to obtain rapid cooling.

V. CONCLUSIONS

Primary carbides provide the hardness required for HSS rolls, but their segregation to cell boundaries is found to deteriorate the fracture toughness. This study has demonstrated that by controlling the alloying elements, the matrix can be modified without changing the volume fraction or the nature of primary carbides. The microstructural modification is especially valuable in large casting such as the HSS rolls because of the difficulty in microstructural modification through cooling-rate control.

In this study, commercially produced HSS rolls have been studied for the improvement of mechanical properties, especially the fracture toughness, by investigating the fracture mechanism in relation to microstructural factors.

(1) The primary carbides are mostly MC types and are segregated to the cell boundaries. As the chromium content increases, the matrices of the HSS rolls are modified from plate-type to lath-type tempered martensite, and more fine spherical carbides are formed in the matrix.
(2) Microcracks initiate either at the primary carbide/matrix interfaces or at primary carbides themselves at relatively low stress-intensity factors, and then readily propagate through adjacent primary carbides. The ductile matrices play a role in retarding the crack propagation.
(3) The fracture toughness and hardness of the HSS rolls depend mostly on the amount and distribution of the coarse primary carbides and depend partly on the characteristics of the matrix.
(4) Roll B displays the highest fracture toughness, attributable to (1) the small cell size and thus the better distribution of primary carbides, (2) the more spherical primary carbides, and (3) the relatively ductile matrix.
(5) In order to improve the overall mechanical properties of the HSS rolls, the homogeneous distribution of the coarse primary carbides must be achieved by reducing the cell size, while the amount of primary carbides must be increased by the optimization of the chemical compositions such as carbon and strong carbide-forming elements.

ACKNOWLEDGMENTS

This work has been supported by Kangwon Industries, Ltd., and the Center for Advanced Aerospace Materials, POSTECH (Korea). The authors thank Professor Nack J. Kim and Dr. Keesam Shin, POSTECH, and Vice President Hee Seung Han, Dr. Hui Choon Lee, and Mr. Young Ik Chun, Kangwon Industries, Ltd., for their helpful discussion on microstructural analysis.

REFERENCES

1. W.F. Smith: *Structure and Properties of Engineering Alloys*, McGraw-Hill, New York, NY, 1981, ch. 1 and ch. 9.

2. W.C. Leslie: *The Physical Metallurgy of Steels*, McGraw-Hill, New York, NY, 1981, ch. 8.
3. R.H. Barkalow, R.W. Kraft, and J.I. Goldstein: *Metall. Trans.*, 1972, vol. 3, pp. 919-26.
4. E.J. Galda and R.W. Kraft: *Metall. Trans.*, 1974, vol. 5, pp. 1727-33.
5. K. Stiller, L.-E. Svensson, P.R. Howell, W. Rong, H.-O. Andren, and G.L. Dunlop: *Acta Metall.*, 1984, vol. 32, pp. 1457-1647.
6. A.-M. El Rakayby and B. Mills: *Mater. Sci. Technol.*, 1986, vol. 2, pp. 175-80.
7. H. Mitsuo, O. Seizi, Y. Kouichiro, K. Kazuo, K. Ryurou, K. Tamotsu, and K. Takahoko: *Iron Steel Inst. Jpn. Int.*, 1992, vol. 32, pp. 1202-10.
8. H. Fredriksson, M. Hillert, and M. Nica: *Scand. J. Metall.*, 1979, vol. 8, pp. 115-22.
9. S. Gongqi, D. Peidao, and Z. Shouze: *Mater. Sci. Technol.*, 1992, vol. 8, pp. 449-54.
10. Henry Wisell: *Metall. Trans. A*, 1991, vol. 22A, pp. 1391-1405.
11. S. Lee, K.-S. Sohn, I.-M. Park, and K.-M. Cho: *Met. Mater.*, 1995, vol. 1, pp. 37-46.
12. Z.-B. Kuang: *Eng. Frac. Mech.*, 1982, vol. 16, pp. 19-33.
13. A.T. Santhanam and R.C. Bates: *Mater. Sci. Eng.*, 1979, vol. 41, pp. 243-50.
14. Robert O. Ritchie, Benjamin Francis, and W.L. Serve: *Metall. Trans. A*, 1976, vol. 7A, pp. 831-52.
15. Y.-H. Kim, D. Kwon, and S. Lee: *Acta Metall.*, 1994, vol. 42, pp. 1887-91.
16. *Standard Test Method for Plain-Strain Fracture Toughness of Metallic Materials*, ASTM E399-83, 1983, ASTM, Philadelphia, PA.
17. D. Broek: *Elementary Engineering Fracture Mechanics*, Martinus Nijhoff Publishers, Dordrecht, The Netherlands, 1983, ch. 8.
18. M.F. Kanninen and C.H. Popelar: *Advanced Fracture Mechanics*, Oxford University Press, New York, NY 1985, ch. 3.
19. E. Haberling, A. Rose, and H.H. Weigand: *Stahl Eisen.*, 1973, vol. 93, pp. 645-51.
20. S. Karagoz, I. Liem, E. Bischoff, and H.F. Fischmeister: *Metall. Trans. A*, 1989, vol. 20A, pp. 2695-2701.
21. T.H. Courtney: *Mechanical Behavior of Materials*, McGraw-Hill Publishing Co., New York, NY, 1990, pp. 169-73.